

## Objective Identification of Cyclones in GCM Simulations

W. KÖNIG

*Meteorologisches Institut der Universität Hamburg, Germany*

R. SAUSEN

*DLR, Institut für Physik der Atmosphäre, Oberpfaffenhofen, Germany*

F. SIELMANN

*Meteorologisches Institut der Universität Hamburg, Germany*

(Manuscript received 2 September 1992, in final form 17 March 1993)

### ABSTRACT

An objective routine for identifying individual cyclones has been developed. The procedure was designed with the aim to keep the input expenditure low. The method ensures a complete collection of cyclones and an exclusion of short time fluctuations attributed to numerical effects. The cyclones are identified as relative minima of the geopotential height field in 1000 hPa. The initial stages of the cyclones are found by locating relative maxima in the 850-hPa vorticity field. Further on the temporal development of the extrema is taken into consideration. An individual cyclone is regarded only if it exists for at least 24 h and if it attains a mature stage at least once, where a certain margin of the geopotential gradient to the surroundings is exceeded.

The identification routine is applied to simulations with the Hamburg general circulation model ECHAM in T21 resolution. Also, cyclone tracks based on ECMWF analyses are evaluated, to which the model results are compared. The effect of different climate conditions, for example, global warming, on cyclone frequency and track location is investigated. It is found that a warmer SST distribution leads to a slight reduction of cyclone frequency in the Southern Hemisphere in fall (March, April, May) and winter (June, July, August); elsewhere the differences are not significant.

### 1. Introduction

Cyclone frequency and the location of major cyclone tracks are important indicators of midlatitude climate. The variability of these parameters on a seasonal time scale has been systematically investigated since the last century (e.g., Van Bebber 1882, 1891), up to a decadal scale in recent years (Reitan 1974; Hayden 1981; John 1990; Zapotocny 1991). These studies, based on manual counting of cyclones, suffer from some subjectivity though the authors were much concerned about homogeneous analyses. Van Bebber (1882) was probably the first who systematically evaluated a large amount of daily weather maps for climatological scope. Cyclones were identified by three synoptic criteria: a local minimum of surface pressure, a pronounced intensity, and a lifetime larger than one day. By these criteria he was able to exclude minor and erratic lows, which contribute about a quarter to the total number of pressure minima. After the manual analysis of cyclones, independently by several meteorologists, the trajectories

were visually condensed to major cyclone tracks. This last step of extrapolation is, however, somewhat questionable. More recent investigations therefore are confined to a presentation of spatial distributions of cyclone frequency. Petterssen (1956) counted the number of cyclone centers over 100 000 km<sup>2</sup> grid areas in the Northern Hemisphere for the period 1899–1939. Klein (1957) used the data of the same period to determine the number of days with lows passing 5° × 5° areas. An improvement of these techniques by Whittaker and Horn (1982) took the trajectories of the cyclones into consideration as well to avoid double counting in the grid boxes. Streaks of maximum frequency were then interpreted as major cyclone tracks.

In recent years a variety of long-term climate simulations with general circulation models have been carried out (e.g., Boer et al. 1984; Washington and Meehl 1984; Manabe and Wetherald 1987; Simmons et al. 1989; Cubasch et al. 1992). The enormous amount of data to be analyzed raised interest in automatic routines for pattern identification. The characteristic features of cyclones or cyclone systems can be traced even in low-resolution models. Thus, methods have been developed for determination of frequency and intensity of cyclone systems or even

*Corresponding author address:* Dr. R. Sausen, DLR, Institut für Physik der Atmosphäre, D-82234, Oberpfaffenhofen, Germany.

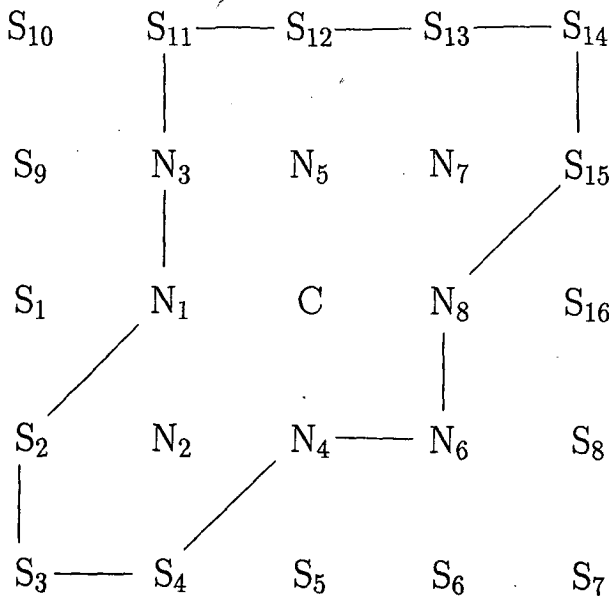


FIG. 1. Example for the identification of a cyclone at grid point C. Position of neighbor ( $N_i$ ) and surrounding ( $S_i$ ) points, which form a closed chain, where the difference of geopotential height exceeds the margin.

individual cyclones in gridpoint fields of a given resolution. These routines must be subject to the following two conditions: first, the pattern recognition should be independent of the geometric shape of the cyclone; second, the computation expense should be kept as low as possible. That means the method should be characterized by universality as well as conciseness to be applicable to large amounts of data in any spatial resolution.

An alternative method for cyclone track climatology has been introduced by locating the variance maxima of the geopotential height in the middle troposphere attributed to disturbances with periods from two days up to a week (e.g., Lau 1988; Trenberth 1991). These streaks, however, must be interpreted as baroclinic waveguides, as Wallace et al. (1988) point out. Some background information about the connection between baroclinic waves and synoptic disturbances is involved to relate the eddy statistics to a storm track climatology. Besides, the structure and evolution of baroclinic waves can vary with geographical location and different climate conditions. A displacement of cyclone centers relative to the anomalies is often found, which is determined in its extent by the climatological mean flow. Moreover, both cyclone and anticyclone tracks contribute equally to the variance field and cannot be satisfactorily distinguished from each other by the bandpass filter. For these reasons it is unlikely that we can infer the tracks of individual cyclones from a knowledge of the bandpass-filtered eddy statistics.

The identification of individual cyclones covers a rather complete climatology of synoptic disturbances.

Among the objective identification routines, the procedure of Williamson (1981) excels in its independence of scale and resolution, though a large amount of mathematical formalism is involved. The method uses a nonlinear least-squares fit to adapt the patterns in the geopotential height field to elliptical structures. By this the discrete gridpoint representation of these patterns is related to their idealized geometrical forms in the continuous space. Though this routine presents an elegant tool for pattern identification, its computational expenditure is rather high, which lessens its value in routine application.

In contrast, Lambert (1988) applied a very simple objective identification routine with low input and computation expenditure. He defined a cyclone as a relative minimum of 1000-hPa geopotential height at a grid point compared to the values at the four neighbor grid points. He put up with some shortcomings including weak spectral fluctuations (Gibbs phenomenon) and lows caused by a reduction to sea level over high terrain. Alpert et al. (1990) proposed a combination of the minimum criterion with a check for the pressure gradient exceeding a certain limit. Thereby the likely original shape of the lows is estimated from a  $2.5^\circ \times 2.5^\circ$  gridpoint resolution by parabolic interpolation. Further on in a square of  $500 \times 500$  km around an identified cyclone center they looked for further minima and only the deepest cyclone was retained.

In our method we refrain from the interpolation between grid points, for the sake of computation time as well as to inhibit restrictions to distinct resolution or special conditions. Nevertheless, the present version of our routine is restricted to data on a Gaussian grid (approximately  $5.6^\circ$  gridpoint distance) of a spectral model with T21 horizontal resolution. This restriction is not essential for the method, but allows dropping some constraints to the identification routine. In a first step, grid points with local minima of geopotential height of 1000 hPa are identified. To avoid an erroneous identification of numerically caused fluctuations we introduce a margin to be exceeded by the height difference between the minimum and selected grid points in its environment. In addition, for a complete representation of the cyclone development in its early stage, we regard a grid point with maximum vorticity at 850 hPa as a possible candidate, if a local geopotential minimum is not found in its surroundings. Section 2 presents the method in detail. In section 3 an application to data of the Hamburg atmosphere climate model ECHAM (Roegner et al. 1992) is shown. A verification is achieved by a comparison with objectively identified cyclones from ECMWF analyses. In section 4 the impact of different climate conditions to cyclone frequency and tracks is studied. The results are based on a coupled ocean-atmosphere simulation (Cubasch et al. 1992). The differences in cyclone fre-

a)

	$l'$	$Z'_t$	$r'_t$				
		$l_t$	$Z_t$	$r_t$			

b)

					$l''_{t+\Delta t}$	$Z''_{t+\Delta t}$	$r''_{t+\Delta t}$
					$l_{t+\Delta t}$	$Z_{t+\Delta t}$	$r_{t+\Delta t}$

c)

			$\hat{l}_{t+\Delta t}$	$\hat{Z}_{t+\Delta t}$	$\hat{r}_{t+\Delta t}$		

d)

		9	4	6	11	14	
		7	$l_{t+\Delta t}$	$Z_{t+\Delta t}$	$r_{t+\Delta t}$	15	
		8	3	5	10	13	

e)

	12	9	4	6	14	17	20
	10	$l_{t+\Delta t}$	$l_{t+\Delta t}$	$Z_{t+\Delta t}$	$r_{t+\Delta t}$	$r_{t+\Delta t}$	21
	11	8	3	5	13	16	19

FIG. 2. Examples of the designation of search regions for checking the temporal continuity of anomalies. (a) Search regions for two anomalies  $Z$  and  $Z'$  at time  $t$ ; (b) search regions for the two anomalies at time  $t + \Delta t$ . Shaded areas resemble locations of the search regions at time  $t$ ; (c) search region at time  $t + \Delta t$  adjacent to two search regions at the preceding time step; (d) order of sequence for check of preceding adjacent search regions, appropriate to 12-h time step (Northern Hemisphere); (e) order of sequence for check of preceding adjacent search regions, appropriate to 24-h time step (Northern Hemisphere).

quency between a run with increasing CO<sub>2</sub> content and a reference run are statistically evaluated.

2. Method

For the identification of atmospheric flow patterns, at least two characteristics are essential: an anomaly in the field of a meteorological variable and some temporal coherence of the feature. To distinguish a certain pattern from similar phenomena, additional criteria must be applied. Small numerically caused fluctuations can usually be discarded by defining a margin for the gradient between the anomaly and its environment. Hence, the spatial extension of the pattern must be defined in accordance to its natural scale and independent of the resolution of the grid. Nevertheless, for simplicity we formulate our method for data on a special spacial and temporal grid. The horizontal grid is the Gaussian grid that is used in T21 spectral models

with a grid spacing of approximately 5.6°. The temporal grid size is preferably  $\Delta t = 12$  h or smaller, but with  $\Delta t = 24$  h the method can also be applied successfully.

Cyclones and cyclonic systems can be directly traced in several lower-level atmospheric fields. We have based our objective identification of cyclones on the check of the following three criteria.

(a) Is there a relative minimum of geopotential height at 1000 hPa, or a relative maximum of vorticity at 850 hPa at a given grid point C?

(b) Is there a stage in the cyclone development in which the difference of geopotential height between the minimum at C and selected surrounding grid points exceeds a certain margin?

(c) Can the pattern be traced for a certain period?

In criterion a for a complete representation of the cyclone development, not only the geopotential height field but

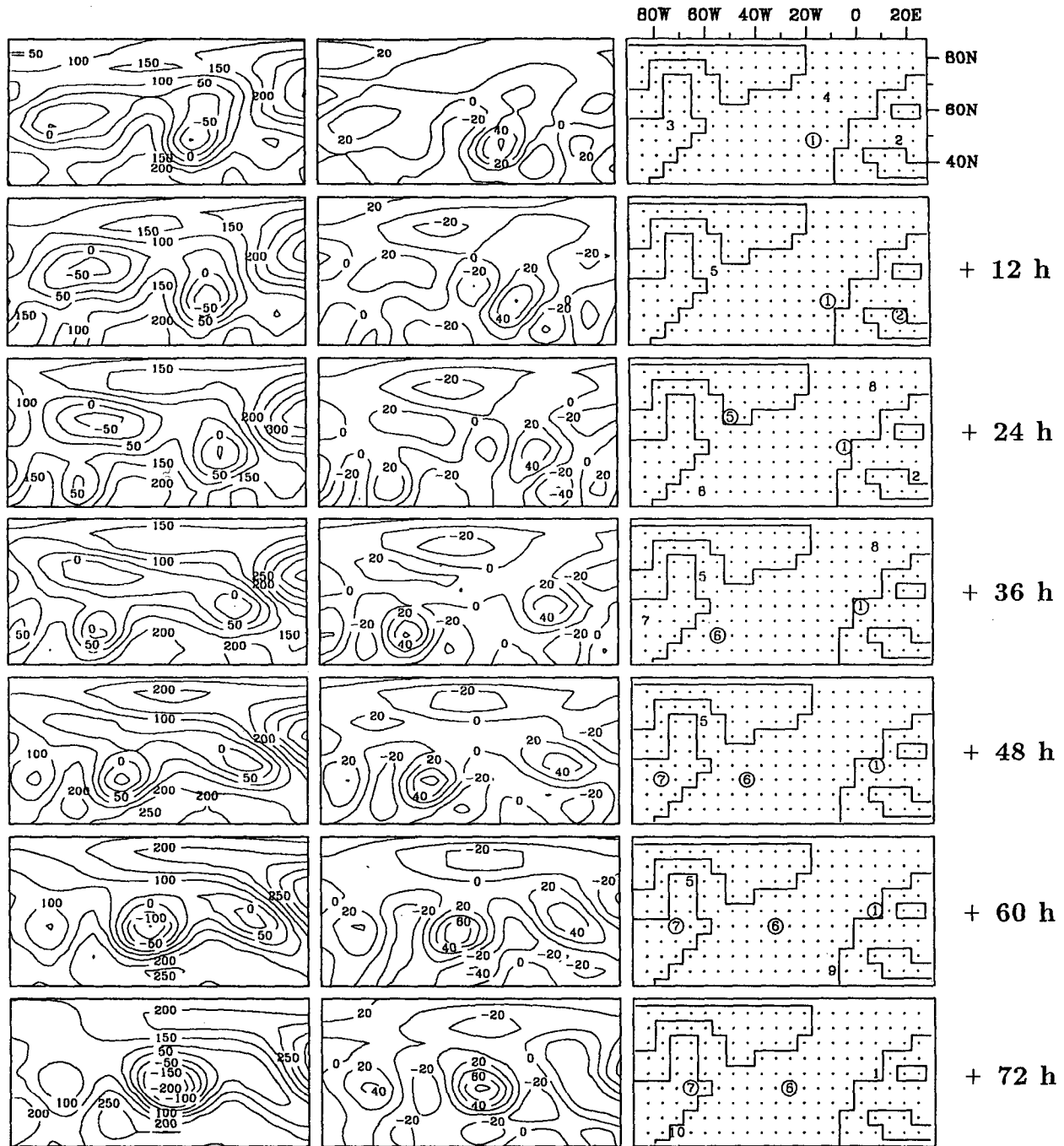


FIG. 3. Sequence of geopotential height fields at 1000 hPa (left), vorticity at 850 hPa (middle), and distributions of identified cyclones (right) over the North Atlantic region for time interval 30 December–6 January, simulation year 10 (forced by SST of January 1977).

also the vorticity field is considered, which represents the early cyclogenesis stages. In the early lifetime a vorticity maximum already exists while a minimum in the geopotential height field has not yet developed.

At least in the mature stage the disturbance should have a gradient of geopotential in its surroundings

greater than a certain limit (criterion b). Thus, a closed chain of grid points with a geopotential height at least 20 gpm higher than the height at C should exist among the 24 neighboring points  $N_i$  and surrounding points  $S_j$  of C (see Fig. 1). This corresponds to a slope of the geopotential height field exceeding 11 gpm/1000 km

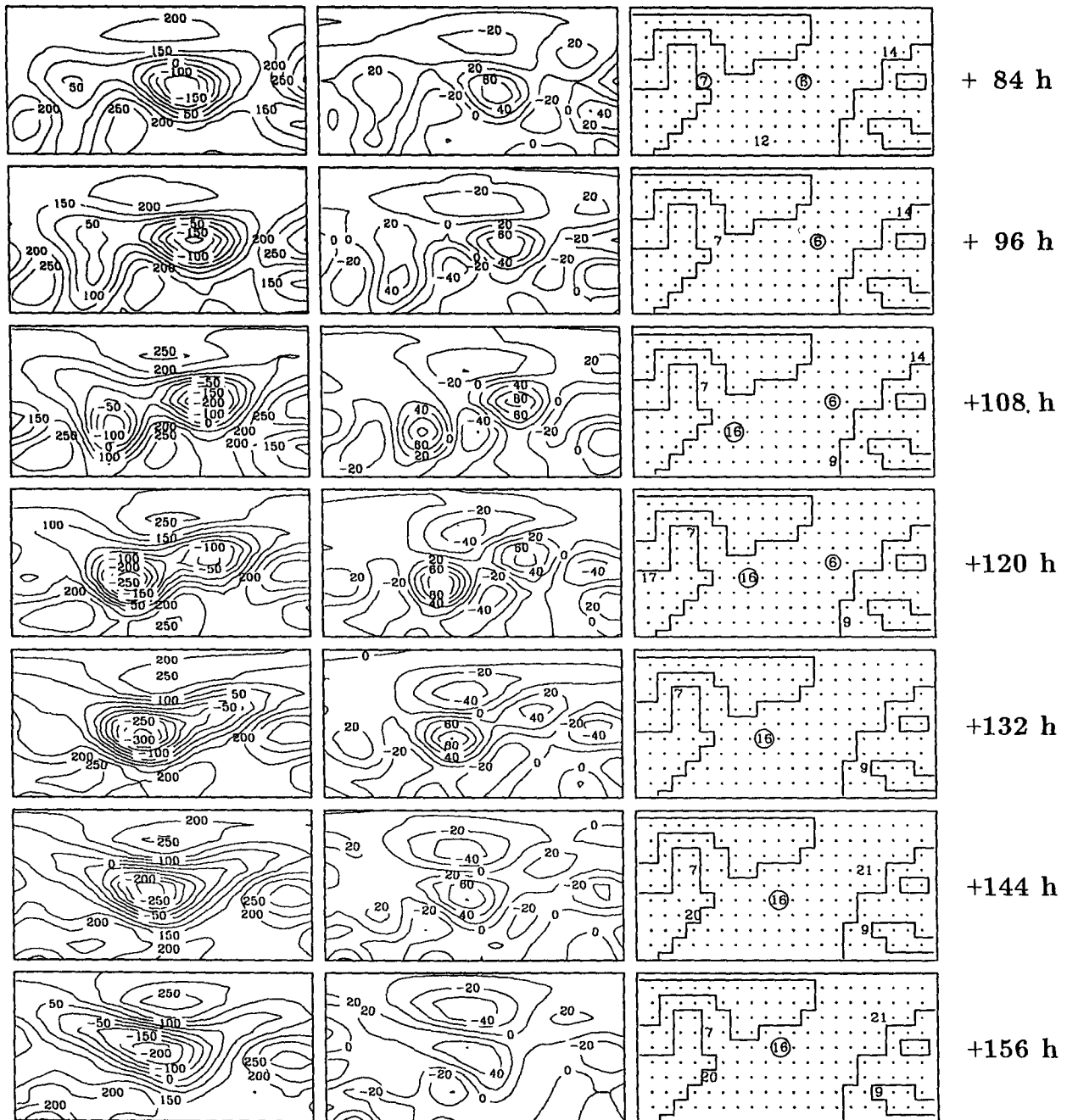


FIG. 3. (Continued) Contours are 50 gpm for geopotential and  $2 \cdot 10^{-5} \text{ s}^{-1}$  for vorticity. In the right plots the ordinal numbers of the traced cyclones are presented. Encircled numbers indicate cases meeting with criterion b.

in any direction. Criterion b inhibits the detection of small (numerically induced) fluctuations in the geopotential height field.

For reasons of numerical efficiency, the check for the closed chain is performed in a two-step procedure. First, only the eight neighboring points  $N_i$  are considered. If the geopotential height difference to C at each point  $N_i$  is at least 20 gpm, a closed chain is detected.

If the test fails at a certain point  $N_i$  (e.g.,  $N_2$  in Fig. 1), we check whether the three surrounding points  $S_j$  adjacent to  $N_i$  (points  $S_2$ ,  $S_3$ , and  $S_4$  in Fig. 1) fulfill the criterion. The numerical value of the margin was ascertained experimentally.

Criterion b need not be fulfilled at every time step of the lifetime of a cyclone. There are surely situations in the early as well as in the decaying stages in which

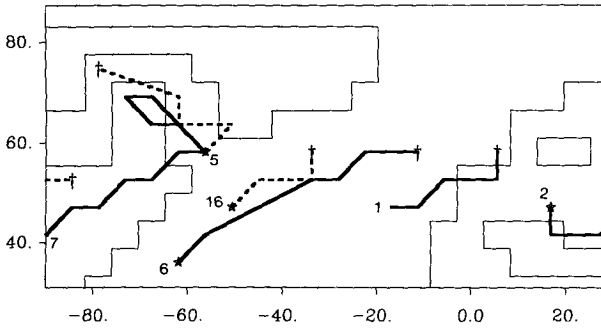


FIG. 4. Trajectories of the identified cyclones over the North Atlantic for the time interval of Fig. 3. A star locates a cyclogenesis, a cross marks the decay state. The ordinal numbers are the same as the cyclone numbers in the right column of Fig. 3. Dashed lines are employed for better distinction of tracks.

the disturbance can become rather weak. The search for the gradient margin is therefore combined with the check of the lifetime of the cyclones. For the model

data with their numerical and resolution deficiencies we require that the cyclone should exist for longer than 24 h. We can then reformulate criterion c:

(c') Can a pattern be uniquely traced by geopotential height minima or vorticity maxima (criterion a) in  $n$  subsequent time steps  $\Delta t$  with  $n \Delta t > 24$  h, and is criterion b fulfilled at least once during this period?

The temporal tracking of cyclones is carried out by specifying search regions around the identified local anomalies and checking for a contact or overlap of these regions within succeeding time steps. Considering the mainly zonal propagation of cyclones as well as taking into account the decrease of gridpoint distance with higher latitudes, the search regions are chosen rectangular with a longer axis in west-east direction. In T21 resolution the region is confined to the adjacent grid points at the same latitude, that is, the search region consists of three grid points. In Fig. 2a two search re-

a)

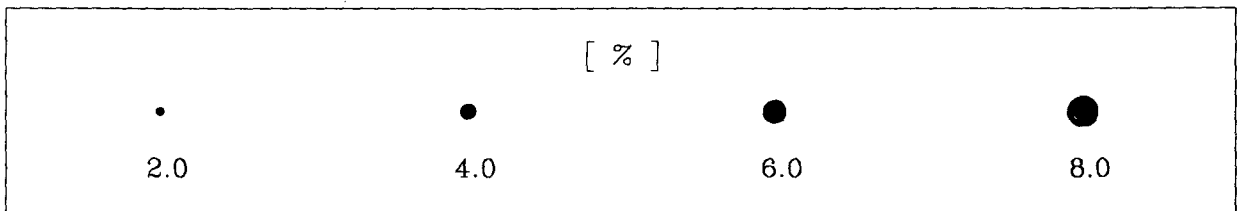
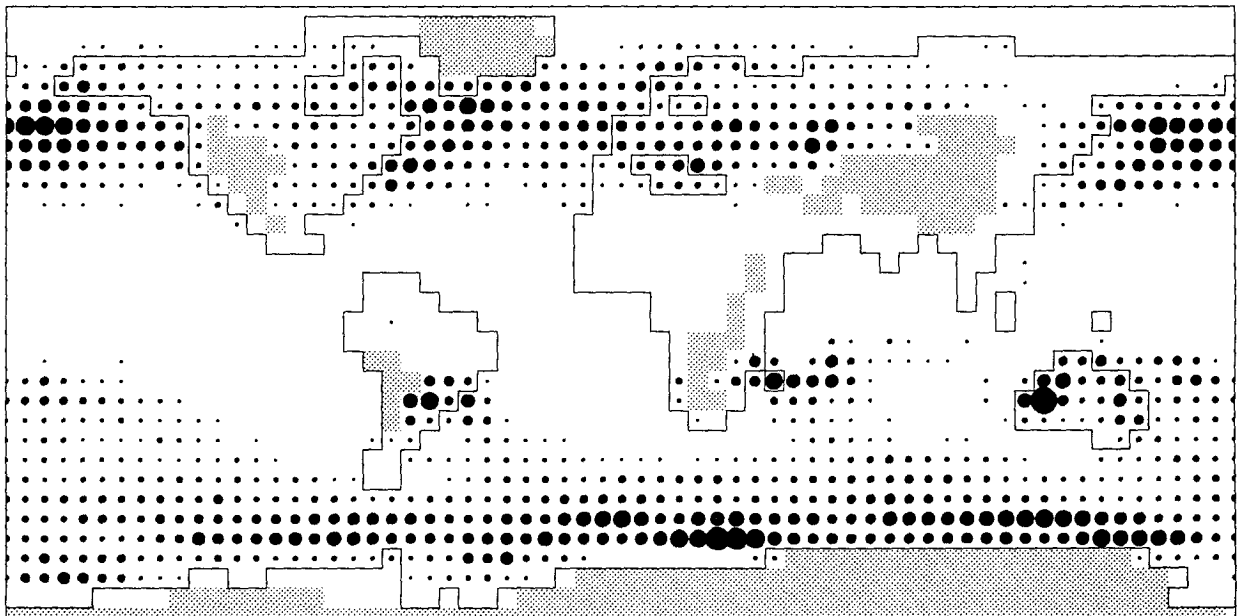


FIG. 5. (a) Mean of seasonal cyclone frequency (i.e., numbers of time steps with cyclones on a grid point divided by number of considered time steps) for boreal winters (December, January, February) of years 1 to 19 of ECHAM2 run. The area of the circles is proportional to the frequency. Circles indicating less than 0.5% frequency are suppressed. (b) Same as (a), but plotted with isolines for better comparison with Fig. 6.

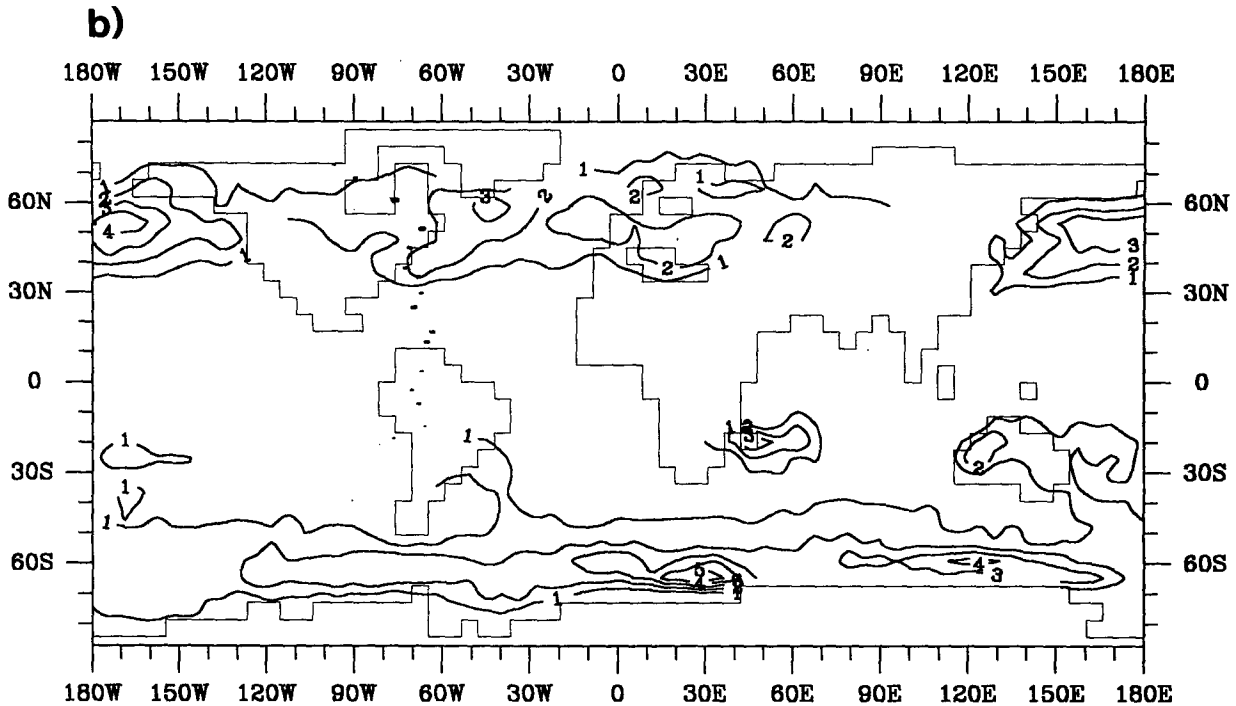


FIG. 5. (Continued)

gions at time  $t$  are indicated by  $(l_t, Z_t, r_t)$  and  $(l'_t, Z'_t, r'_t)$ , where  $Z_t$  and  $Z'_t$  indicate the cyclone centers,  $l_t, l'_t$  and  $r_t, r'_t$  the left and right neighbors, respectively. The tracing of individual cyclones is then carried out in the following manner.

Each height minimum and/or vorticity maximum (cyclone center) at time  $t$  gets a certain ordinal number ( $Z_t$  and  $Z'_t$  in Fig. 2a). The left and right neighbor grid points  $[(l_t, r_t, l'_t, r'_t)]$  in Fig. 2a] of the cyclone centers receive the same number as the latter, that is,  $l_t = r_t = Z_t$  and  $l'_t = r'_t = Z'_t$ . If at the same time  $t$  two search regions are overlapping or adjacent, that is, the distance between the two regions is equal to or less than one grid size, both regions are combined in one region with the same ordinal number; the point with the lowest geopotential height is regarded as the cyclone center. Then the field is examined for the following time step  $t + \Delta t$ . In Fig. 2b, the search regions at time  $t + \Delta t$  are indicated by  $(l_{t+\Delta t}, Z_{t+\Delta t}, r_{t+\Delta t})$  and  $(l''_{t+\Delta t}, Z''_{t+\Delta t}, r''_{t+\Delta t})$ . The geographic position of the search regions at time  $t$  is indicated by shading. A search region at time  $t + \Delta t$  can be associated with a search region at time  $t$  if the spatial distance of the two regions is equal or less than the grid size, either in meridional or longitudinal direction. In that case the search region at time  $t + \Delta t$  gets the same ordinal number as the region at time  $t$  it was associated with. Otherwise it receives a new number. In the case of Fig. 2b, the region  $(l_{t+\Delta t}, Z_{t+\Delta t}, r_{t+\Delta t})$  can be associated with the region  $(l_t, Z_t,$

$r_t)$  of Fig. 2a, thus  $Z_{t+\Delta t} = Z_t$ , that is, the cyclones with the centers at grid boxes indicated by  $Z_{t+\Delta t}$  and  $Z_t$  are regarded as the same cyclone at different time steps. The region indicated by  $(l''_{t+\Delta t}, Z''_{t+\Delta t}, r''_{t+\Delta t})$  cannot be associated with a predecessor region at time  $t$ . Thus, its center is regarded as the center of a new cyclone, and  $Z''_{t+\Delta t}$  gets a new ordinal number.

It may happen that a search region at time  $t + \Delta t$  is close to more than one region at time  $t$  (such a situation is plotted in Fig. 2c). In order to guarantee that a search region is associated with at most one predecessor search region, the search for that predecessor is performed in a certain order. The order is based on the observational finding that cyclones in extratropics move predominantly eastward. In detail the search for a predecessor of a search region at time  $t + \Delta t$  [indicated by  $(l_{t+\Delta t}, Z_{t+\Delta t}, r_{t+\Delta t})$ ] is performed in the following way (Fig. 2d). For the 15 grid boxes covered by and adjacent to the search region, it is checked whether some of these grid boxes are also covered by a search region at time  $t$ . The check is performed in the order indicated by the numbers in Fig. 2d. As soon as the test is positive for the first time, the search is stopped and the region at time  $t + \Delta t$  is associated with the detected region at time  $t$ .

After the application of the method to the whole time series, trajectories of the cyclones can be drawn by linking the centers of regions with the same ordinal number. Here the time filter of criterion  $c'$  is applied.

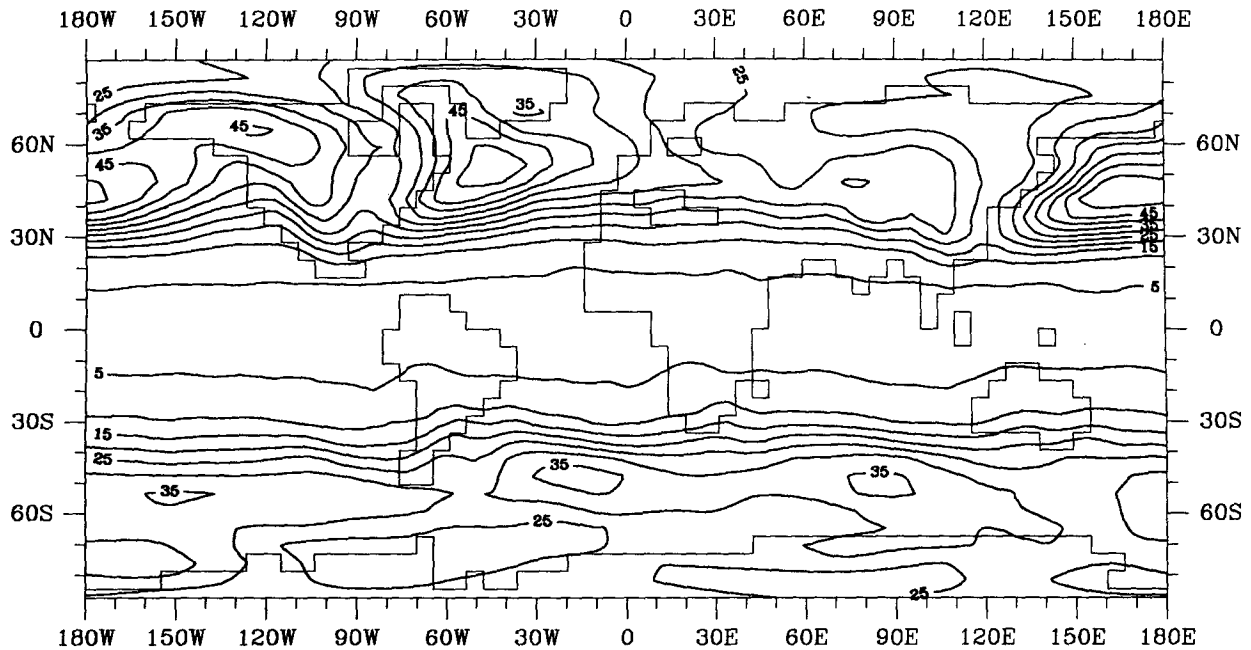


FIG. 6. Mean of bandpass-filtered standard deviation of geopotential height in 1000 hPa for boreal winters of years 1 to 19 of ECHAM2 run. The contour interval is 5 gpm.

Only those patterns are retained that exist for longer than 24 hours. Those cyclones that never fulfill criterion b are then eliminated.

Once the cyclones and their trajectories are detected, stationary and traveling cyclones can easily be distinguished. Here we define a stationary cyclone as a cyclone whose center is at the same position during its whole lifetime.

In order to avoid errors due to the reduction of the surface pressure at high terrain to sea surface level, areas with high orographic elevation over 1000 m are ignored in our procedure. In this area erroneous persistent anomalies of the 1000 hPa height field could sometimes be detected.

Our method is illustrated by an example in Fig. 3. From a GCM simulation in T21 horizontal resolution a sequence of 14 subsequent fields with a time step of 12 h has been arbitrarily selected. At each time step the 1000-hPa geopotential height field (left column) and the 850-hPa vorticity (middle column) have been plotted for a selected region (North Atlantic Ocean). In the right column the model grid points are indicated by dots and the ordinal number of each geopotential minimum or vorticity maximum is plotted regardless of criteria b and c' being met or not. When an anomaly passes criterion b, the number is encircled. Finally the validity of criterion c' is checked. Criterion c' is fulfilled if the same cyclone occurs in at least three subsequent rows of Fig. 3. Weak disturbances and cyclones of duration shorter than 24 h are dropped. Only the cyclones with the numbers 1, 2, 5, 6, 7, and 16 remain. In Fig.

4 the tracks of the remaining cyclones appearing in the selected area and time interval are plotted (including cyclones starting or ending outside the area or time interval).

This case study shows an example of cyclones over the North Atlantic in a seven-day period from 30 December to 6 January (each model month consists of 30 days). One major disturbance can be traced from its origin as a vorticity maximum at the east coast of North America to the decay phase in the eastern Atlantic (ordinal number 6). Over northern Europe an intense high prevents the cyclones from traveling farther eastward. Besides the west-east track over the ocean some weaker disturbances take a path from the North American continent through Davis Strait up to the north (ordinal numbers 5, 7). This path as well as the North Atlantic track correspond pretty well to major climatological tracks recorded by Whittaker and Horn (1982), only the decay of the disturbances happens a bit earlier than suggested from the climatology.

### 3. Application to a GCM simulation

In this section the capability of the identification routine is investigated. A comparison with the statistics of the bandpass-filtered variance of geopotential height is carried out. The cyclone identification for observed data is also presented. How much the routine depends on an appropriate temporal resolution is also checked. With these investigations two aspects of validation, the

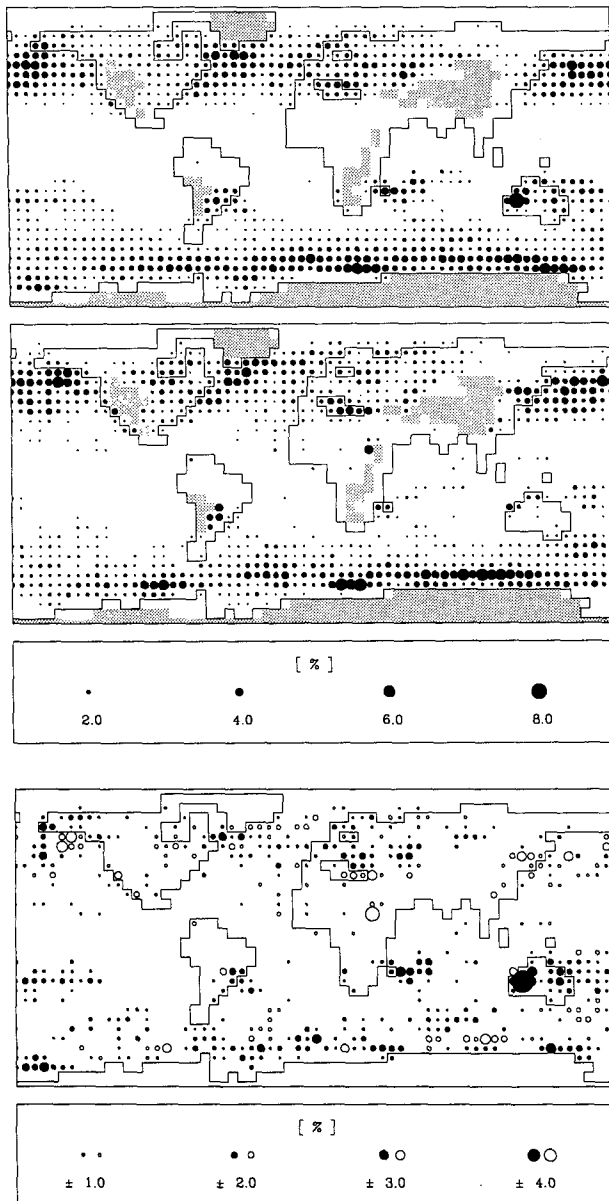


FIG. 7. Mean of seasonal cyclone frequency for boreal winters. Upper panel: ECHAM2, years 12/13–18/19; middle panel: ECMWF analyses, 1983/84–1989/90; lower panel: difference model minus observation. The difference plot uses a different scale. Open circles indicate negative values. Otherwise same as in Fig. 5.

reproduction of physical mechanisms and the stability with time step variation, are illustrated.

The model data (achieved with  $\Delta t = 12$  h), which we analyze in this section, have been generated with the Hamburg atmosphere general circulation model ECHAM2 (Roeckner et al. 1992). This model is based on the ECMWF numerical weather forecast model. The parameterizations of the subgrid physical processes were modified to be more appropriate for climate modeling. In addition to vorticity, divergence, tem-

perature, surface pressure, and humidity, the cloud water (liquid and solid phase) is a prognostic variable. The model simulation analyzed in this section was performed at T21 horizontal resolution. The daily and annual cycles were included. Monthly varying fields of the observed sea surface temperature of the period 1970–1988 were prescribed.

The occurrence of cyclones over a certain grid point is measured by the cyclone frequency, that is, the ratio of the number of positive events according to the above-mentioned criteria to the total number of investigated time steps. Contrary to Alpert et al. (1990) a cyclone is counted  $n$  times if the same cyclone appears for  $n$  time steps at the same grid point. This gives large weight to stationary cyclones. To dampen this deficiency, solely stationary anomalies, that is, cyclones that stay at the same grid point for their whole lifetime, were not counted in our frequency plots. These systems were, anyhow, mostly confined to the tropics. The cyclone counting was applied to model data from the ECHAM2 simulation mentioned above (Fig. 5) and compared with results of the bandpass-filtered (2.5–6 d) fluctuations of the geopotential height field in 1000 hPa (Fig. 6). The streaks of enhanced cyclone frequency in Fig. 5 coincide well with the known major climatological cyclone tracks (e.g., see Whittaker and Horn 1982; Taljaard 1972). The locations of cyclone activity over the western North Atlantic, over the North Pacific, and in the Southern Hemisphere's roaring forties are well represented. A similarity to the features of the bandpass-filtered geopotential variances (Fig. 6) is evident. The maxima of the bandpass variances are found farther equatorward than the highest cyclone frequencies, in accordance to the investigations of Wallace et al. (1988). Further, some local discrepancies occur. This especially concerns the waveguide over northwestern Canada, which is less represented by the pattern identification routine. In fact, many of the lows in this region are rather weak and are therefore dropped by criterion b. On the other hand, the cyclone tracks extending from the southern subtropical continents to the roaring forties cannot be reproduced by the bandpass analysis. This method utilizes deviations from the climatological mean and is therefore not capable of identifying all disturbances if the climatological mean is low. Further, the bandpass interval in the Southern Hemisphere is different from that in the Northern Hemisphere (Trenberth 1991). This could not be considered in the analysis presented in Fig. 6.

Another peculiarity appears in a cyclone frequency maximum over west Australia. Here, a deficiency of the ECHAM2 model simulation gives the reason. An overestimation of the land–sea contrast in the model leads to strong temperature gradients, and quasi-stationary cyclonic flow. By inspection of the daily maps we frequently found heat lows over northwest Australia that suffered only slight displacements.

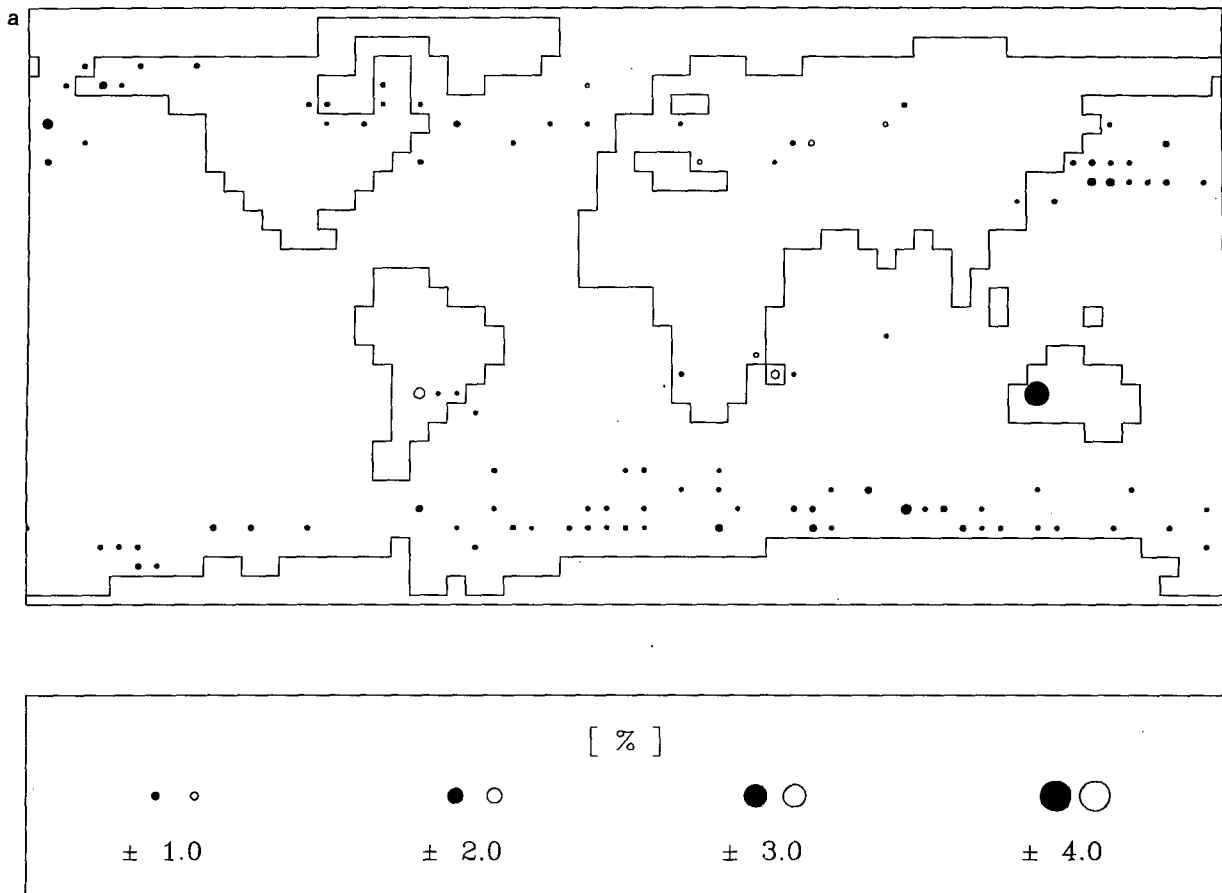


FIG. 8. Difference of mean seasonal cyclone frequency for boreal winters of years 1–19 of ECHAM2 run between (original) 12-h temporal resolution and (thinned out) 24-h resolution. (a) Global distribution, (b) a section of the North Atlantic region ( $90^{\circ}\text{W}$ – $30^{\circ}\text{E}$ ,  $30^{\circ}\text{N}$ – $87^{\circ}\text{N}$ ). Open circles indicate negative differences. In (a) the circles amounting to less than 0.5% are suppressed. The stippled area in (b) marks the region where cyclone frequency exceeds 2%.

We also compared the model data with ECMWF analyses truncated to T21 resolution. For a fair comparison we restricted the model data to almost the same period as the ECMWF data available to us, that is, the seven boreal winters 1981/82–1987/88 in the model were compared to observations of 1983/84–1989/90. In Fig. 7 the global distribution of mean cyclone frequency simulated with ECHAM2 and that of the ECMWF analyses are shown. (Despite the fact that Fig. 7, top panel, is based on a subset of the data used to construct Fig. 5, both figures are quite similar.) The location of the major cyclone tracks agrees quite well between model run and observations. The difference pattern (lower panel) reveals only minor discrepancies, which are partly caused by model deficiencies, such as the absence of the Alps or again the overestimation over west Australia. Other differences, for example, in the South Atlantic or in the Indian Ocean, are probably due to lack of observations.

Unfortunately the ECMWF data available to us had only a 24-h time stepping. Thus, the differences be-

tween the analyses and the model results could also stem from a diverging performance of the identification method with a different temporal resolution of the data. For a check of the effect of various time steps the routine was applied to ECHAM2 data, which were artificially thinned out to a 24-h time step, and compared with the results of the complete ECHAM2 dataset. The difference between identifications of 12- and 24-h data is presented in Fig. 8. The global distribution shows only minor discrepancies. The only outstanding difference over west Australia reveals that the cyclones in this region are indeed not stationary systems. The 12-h data catch up with the development of these cyclones, while the 24-h data often cannot be assigned to an uninterrupted sequence. For a further illustration a section of the North Atlantic is selected (Fig. 8, lower panel). Major cyclone tracks are identified, where the cyclone frequency exceeds 2%. It can be seen from Fig. 5 that the regions with frequencies exceeding this margin fairly resemble the typical courses (Whittaker and Horn 1982). Over the majority of grid points the cy-

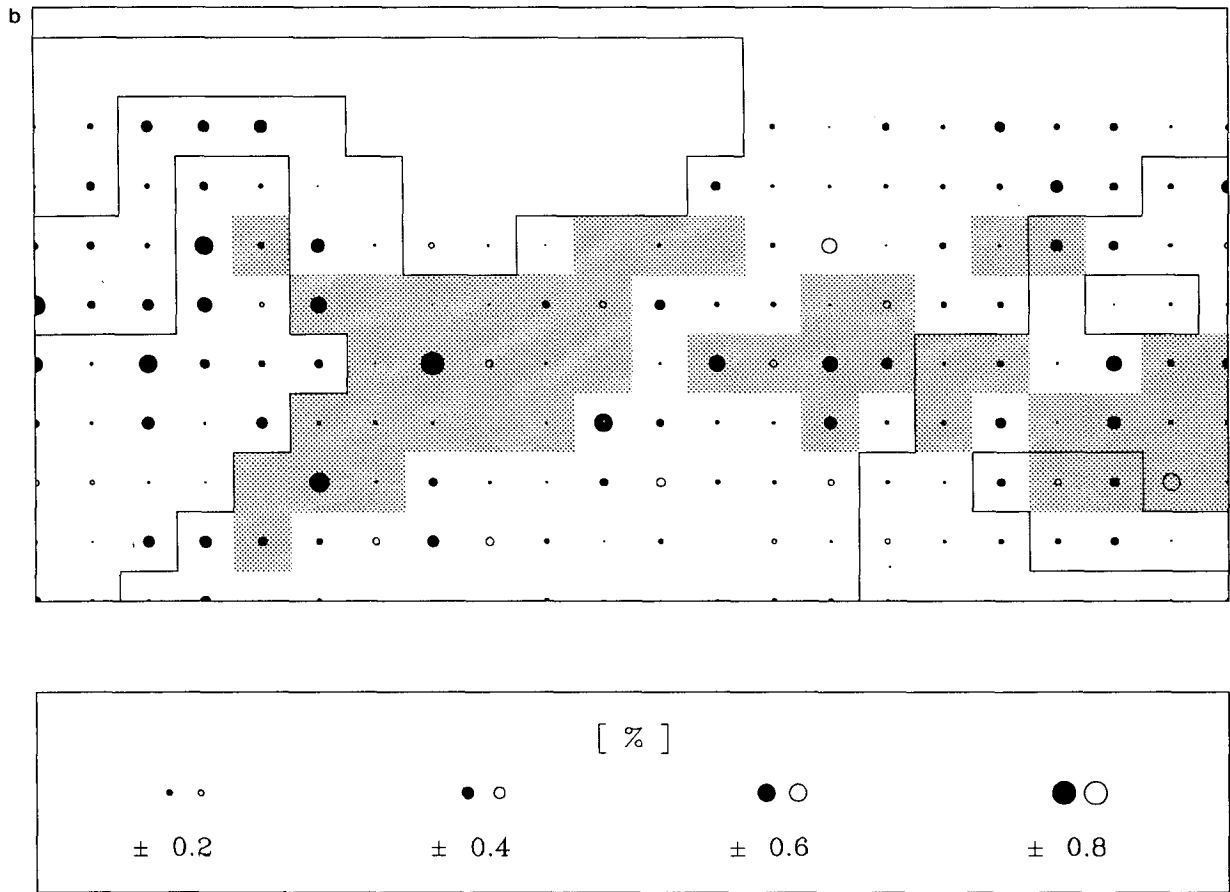


FIG. 8. (Continued)

clone frequencies of the 12-h data slightly exceed those of the daily fields. This means that with a time step of 24 h some anomalies cannot be connected to coherent tracks. The few differences bigger than 0.5%, however, are mostly confined to the region of high cyclone frequency or to its edges. The enhanced occurrence of positive differences over northeastern Canada indicates a minor cyclone track (cf. Whittaker and Horn 1982), which is better resolved with a 12-h time step. In general the difference between 12- and 24-h data identification is about one order of magnitude smaller than the frequency distributions themselves. A comparability of the 24-hourly ECMWF analyses with the 12-hourly ECHAM2 model results is therefore guaranteed.

**4. Impact of global warming**

As an effect of anthropogenic climate modification, the influence of a warming of the atmosphere due to increased CO<sub>2</sub> concentration has been investigated by Cubasch et al. (1992). Four simulations, each extending on 100 years of simulated time, have been performed with different scenarios of the equivalent CO<sub>2</sub> concentration. Two of these scenarios will be analyzed

here: Intergovernmental Panel on Climate Change (IPCC) scenario A, which assumes an equivalent CO<sub>2</sub> increase of 1.3% per year, and control, where the equivalent CO<sub>2</sub> concentration is kept constant at the value of 1985. In the control simulation the global near-surface temperature exhibits only little change; during the 100 years of simulated time it drops by only 0.4 K. Due to a cold-start retardation (Hasselmann et al. 1993), the global-mean near-surface temperature increases by only 0.3 K during the first three decades of scenario A but then shows a more rapid growth and reaches a value 2.6 K higher than the initial value after 100 years. For our investigations we concentrate on the last decades of the two simulations (years 91–100). We have analyzed the cyclone frequency. Figure 9 shows the result for all seasons. At first view, a slight decrease of cyclone frequency in the warm climate is noticed, which is consistent with a reduction of the meridional temperature gradient at the surface. For fall and winter the difference patterns over the North Atlantic reveal that especially at the equatorward edges of the major tracks the cyclonic activity is reduced in scenario A, while the frequency at the poleward edges is increased. These two features correspond to a pole-

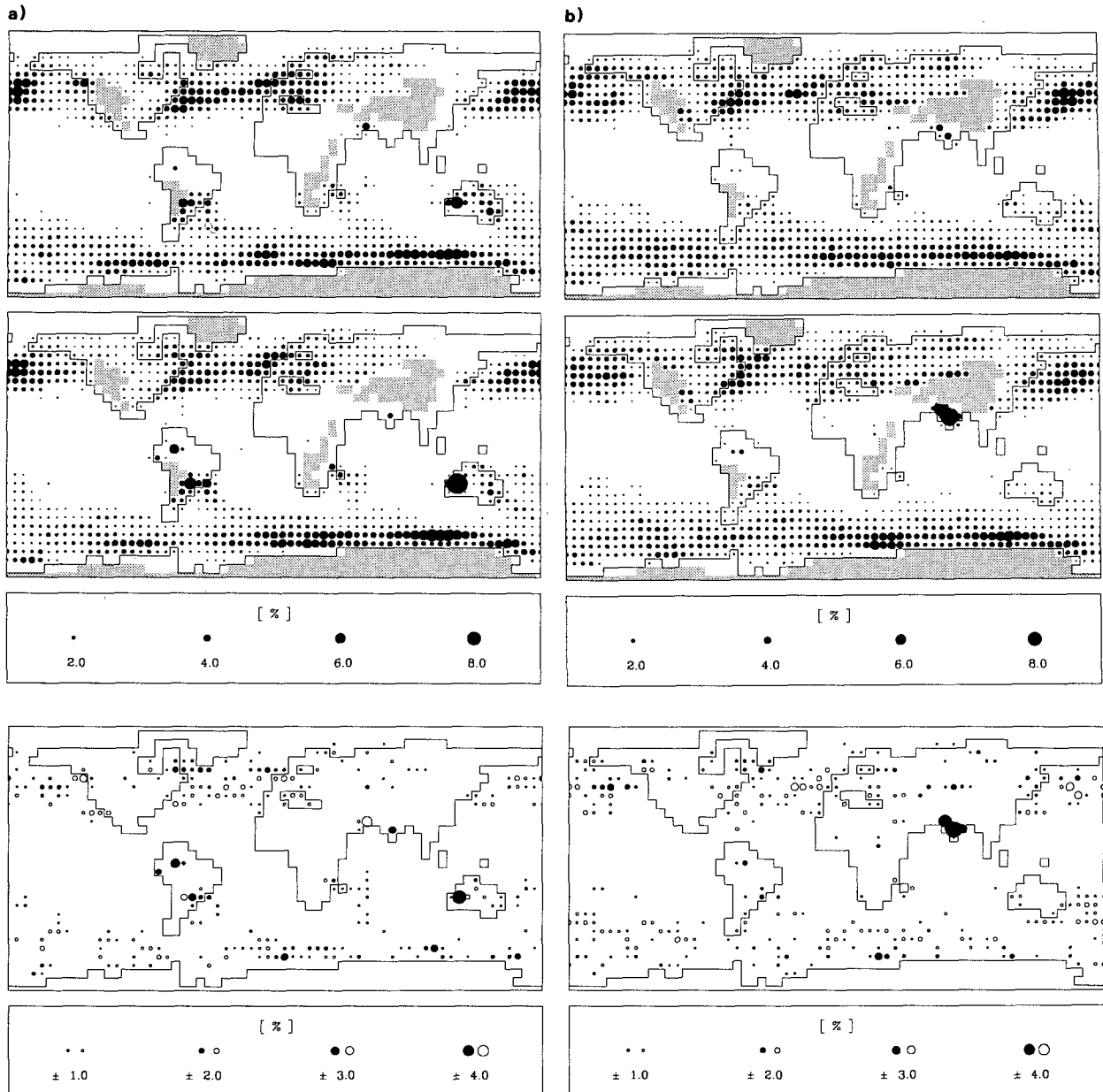


FIG. 9. Mean cyclone frequency for seasons of years 91–100 for runs with a coupled ocean–atmosphere model (ECHAM + LSG). Upper panel: control climate; middle panel: scenario A climate; lower panel: scenario A minus control. Open circles indicate negative differences. Otherwise same as in Figure 5. (a) December, January, February, (b) March, April, May.

ward shift of the major cyclone tracks as was expected with a warming of the midlatitude climate. A similar tendency is observed over extended regions of the Southern Hemisphere. Over the North Pacific a rather eastward displacement of the frequency maximum is noticed, especially in winter and spring. In boreal summer the distribution tends to become patchy with the warmer climate, an indication that the cyclone tracks become shorter due to lack of baroclinity.

In the tropical atmosphere some other effects become obvious by the identification procedure, such as an in-

creased persistence of the west Australian heat low in boreal winter and the development of a similar phenomenon over the Amazon region in boreal fall, winter, and spring. The increase of cyclone frequency over India, beginning in boreal winter and drastically expanding in boreal spring, suggests that the onset of monsoon comes earlier in the warmer climate.

The statistical significance of the differences is checked by a Wilcoxon rank test (Sachs 1968) for selected regions, such as the northern extratropics ( $42^{\circ}\text{N}$ – $76^{\circ}\text{N}$ ), within this belt separately for the Atlantic

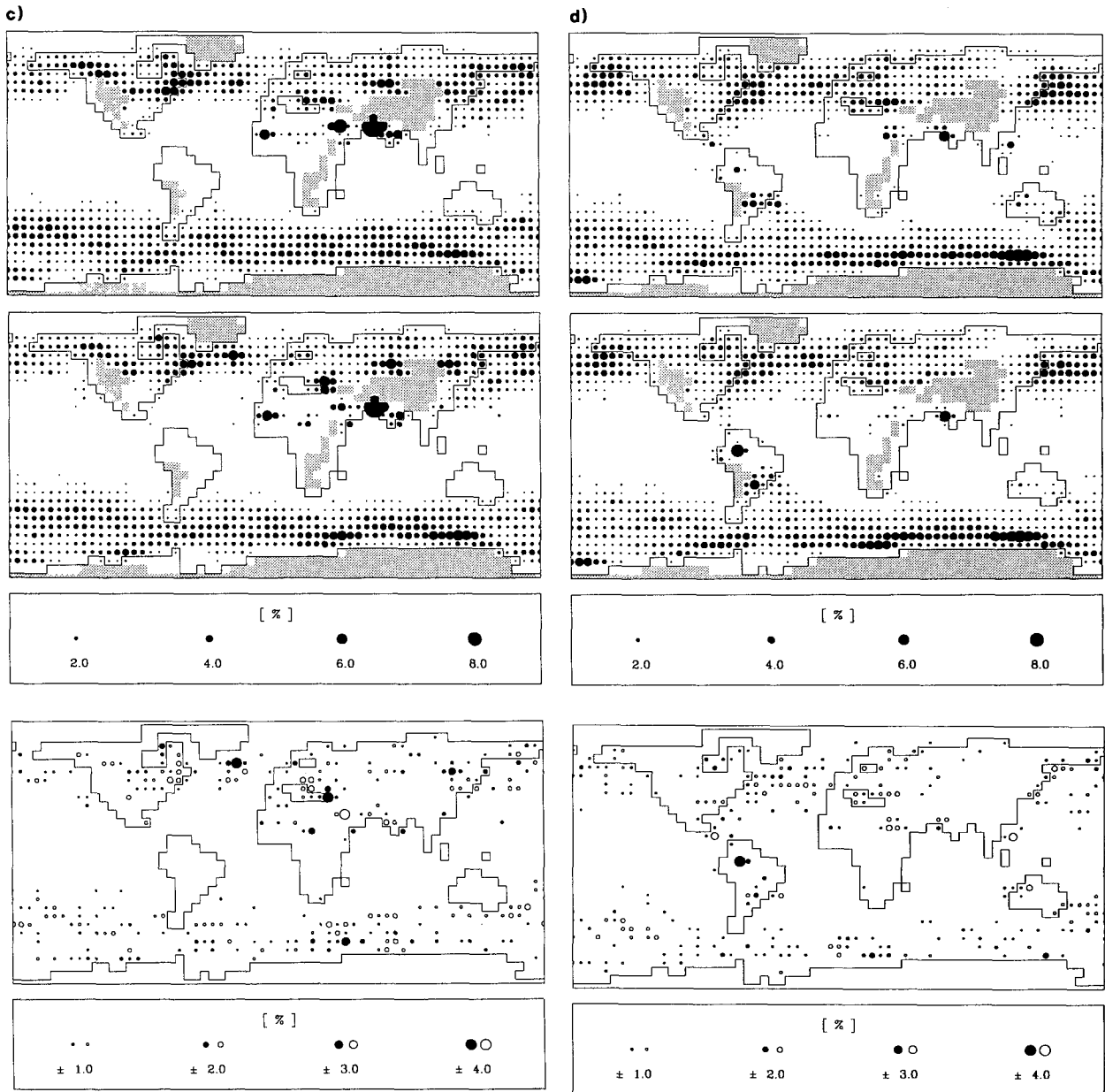


FIG. 9. (Continued) (c) June, July, August, (d) September, October, November.

(95°W–25°E) and Pacific regions (123°W–113°E), and southern extratropics (37°S–70°S), respectively. The distribution-independent procedure yields characteristic measures of the overall difference of cyclone frequency between scenario A and reference run for the four seasons (Table 1). The numbers describe the distance between the distribution peaks, regardless of sign. Thus, the multivariate check only indicates the figure of the difference between scenario A and the reference run. The sign of the difference is revealed only by a comparison of the cyclone frequency distributions. The percentages represent the significance

levels of the differences. It is obvious that in the southern belt the differences are more significant than those of the northern extratropics in the respective seasons. The rather low significance levels in the Northern Hemisphere are related to a low cyclone frequency over the continents, but also to a limitation of differences to distinct regions over the oceans. Except in winter, the differences over the North Atlantic are a bit more significant than those over the northern Pacific, probably due to the larger extension of negative differences. The 99% significance level is only achieved in the Southern Hemisphere's cyclone belt during fall and

TABLE 1. Wilcoxon characteristic values and corresponding significance levels of cyclone frequency differences between scenario A and control tenth decade for selected regions in seasons DJF, MAM, JJA, SON.

	DJF	MAM	JJA	SON
Northern extratropics	0.61	0.84	0.67	1.12
42°N–76°N	50%	80%	50%	80%
Northern Atlantic	1.60	1.29	0.78	1.43
42°N–76°N, 95°W–25°E	90%	90%	50%	90%
Northern Pacific	1.63	1.09	0.75	1.21
42°N–65°N, 123°E–113°W	90%	80%	50%	80%
Southern extratropics	1.49	2.77	2.41	1.58
37°S–70°S	90%	99%	99%	90%

winter, when the cyclone activity attains its maximum. In these seasons a shift of cyclone frequency to the South Pole is most clearly expressed.

We also carried out investigations on the frequency of cyclone classes of different intensity, that is, different thresholds for criterion b. Partly due to the smaller sample sizes, no significant differences could be detected between scenario A and the control run.

## 5. Conclusions

An objective identification routine for individual cyclones was presented. It consists of three steps: a localization of a geopotential height minimum at 1000 hPa, a check on the depth of this minimum exceeding a special margin, and an examination of the preceding stages with vorticity maxima at 850 hPa, as well as the decaying stages with weak geopotential anomalies. The power of the procedure lies in its ability to separate disturbances of different intensities. For this purpose the investigation is based on the absolute fields rather than on the anomalies. Therefore the method yields a supplementary view to other tools of storm track identification, for example, investigation of bandpass-filtered eddy statistics.

Due to model resolution the amount of cyclone frequency is much lower than that of former manual analyses. However, the global distribution as well as the local enhancement of cyclone occurrence along the major cyclone tracks match quite well to the climatologies recently published.

An investigation of the temporal tracking of the identification routine was carried out with two different temporal resolutions of the same data. A slight sensitivity to the length of the time step was noticed. A realistic representation of the actual cyclones is achieved if the relationship of identification radius to time step hits the actual propagation velocity of the cyclones.

The finer the temporal and spatial resolution, the better the results of the cyclone identification should be. A time step of 24 h can give a fairly reasonable record of the temporal development of a cyclone.

However, for a good performance, a 12-h resolution should be envisaged.

We are aware of the fact that a repeated counting of temporarily stationary anomalies can lead to some bias in the frequency distribution. This should be especially evident in regions of cyclolysis. In our results, however, a clustering of frequency could not be identified in typical decay regions. We infer that such biases play only a minor role in a sufficiently large dataset.

Despite some deficiency in cyclone identification from 24-hourly observations, the ECMWF analyses and the model data show a good agreement over the Northern Hemisphere. There are some discrepancies in the tropics and over the southern extratropics, where the model underestimates the cyclone activity in the “roaring forties” region. The differences are, however, subject to defects of the model simulations rather than to the identification procedure itself.

The effect of global warming on the cyclone activity is globally more significant in the Southern Hemisphere. In the Northern Hemisphere some weaker differences between scenario A and the control run occur, especially in winter, and result in a northward shift of the major cyclone track in the North Atlantic and an eastward shift of the frequency maximum in the North Pacific.

In general, the objective identification routine of individual cyclones offers a comfortable and economic tool for the study of the sensitivity of baroclinic activity on different climate conditions. As a phenomenological method it is superior to physical concepts, which often depend on theoretical presuppositions. Because the routine is flexible, it allows further extensions, for example, for the investigation of spectra of cyclone intensity.

The computational expenditure on a Cray-2S amounts to about 20 sec for the investigation of one month of 12-hourly data. About two-thirds of this time is spent in tracing the cyclones.

*Acknowledgments.* This study was supported by the Commission of the European Communities through Grant EV4C-0031-D, by the German Federal Ministry of Research and Technology (BMFT) through Grant 07 KFT 05/6 and by Deutsche Forschungsgemeinschaft within division SFB 318. The authors are grateful to Dr. Michael Ponater, who provided the bandpass analyses as a base for Fig. 6. We would also like to thank the anonymous reviewers for their helpful comments. Thanks are due to Ms. Karin Niedl for preparing the manuscript.

## REFERENCES

- Alpert, P., B. U. Neeman, and Y. Shay-El, 1990: Climatological analysis of mediterranean cyclones using ECMWF data. *Tellus*, **42A**, 65–77.
- Boer, G. J., N. A. McFarlane, and R. Laprise, 1984: The Climatology of the Canadian Climate Centre general circulation model as

- obtained from a five year simulation. *Atmos. Ocean*, **22**, 430–475.
- Cubasch, U., K. Hasselmann, H. Höck, E. Maier-Reimer, U. Mikolajewicz, B. D. Santer, and R. Sausen, 1992: Time-dependent greenhouse warming computations with a coupled ocean-atmosphere model. *Climate Dyn.*, **8**, 55–69.
- Hasselmann, K., R. Sausen, E. Maier-Reimer, and R. Voß, 1993: On the cold start problem in transient simulations with coupled atmosphere-ocean models. *Climate Dyn.*, in press.
- Hayden, B. P., 1981: Secular variation in Atlantic coast extratropical cyclones. *Mon. Wea. Rev.*, **109**, 159–167.
- John, J. I., 1990: Secular changes in storm tracks over the North Atlantic Ocean, 1920–1989. *Symp. on Global Change Systems. Special Sessions on Climate Variations and Hydrology*, Anaheim, Amer. Meteor. Soc., 164–166.
- Klein, W. H., 1957: Principal tracks and mean frequencies of cyclones and anticyclones in the Northern Hemisphere. Res. Pap. No. 40, U.S. Weather Bureau, Washington D.C., 60 pp.
- Lambert, S. J., 1988: A cyclone climatology of the Canadian Climate Center general circulation model. *J. Climate*, **1**, 109–115.
- Lau, N.-C., 1988: Variability of the observed midlatitude storm tracks in relation to low-frequency changes of the circulation pattern. *J. Atmos. Sci.*, **45**, 2718–2743.
- Manabe, S., and R. T. Wetherald, 1987: Large-scale changes of soil wetness induced by an increase in atmospheric carbon dioxide. *J. Atmos. Sci.*, **44**, 1211–1235.
- Petterssen, S., 1956: *Weather Analysis and Forecasting*, Vol. 1. 422 pp.
- Reitan, C. H., 1974: Frequencies of cyclones and cyclogenesis for North America. 1951–1970. *Mon. Wea. Rev.*, **102**, 861–868.
- Roeckner, E., K. Arpe, L. Bengtsson, S. Brinkop, L. Dümenil, M. Esch, E. Kirk, F. Lunkeit, M. Ponater, B. Rockel, R. Sausen, U. Schlese, S. Schubert, and M. Windelband, 1992: Simulation of the present-day climate with the ECHAM model: Impact of model physics and resolution. Max-Planck-Institut für Meteorologie. Report No. 93, 171 pp. [available at MPI für Meteorologie, Bundesstr. 55, D-20146, Hamburg, Germany.]
- Sachs, L., 1968: *Statistische Auswertemethoden*. Berlin, Heidelberg, 293–302.
- Simmons, A. J., D. M. Burridge, M. Jarraud, C. Girard, and W. Wergen, 1989: The ECMWF medium-range prediction models, development of the numerical formulations and the impact of increased resolution. *Met. Atmosph. Phys.*, **40**, 28–60.
- Taljaard, J. J., 1972: Synoptic meteorology of the southern hemisphere. *Meteorology of the Southern Hemisphere, Meteor. Monogr.*, No. 13, H. van Loon, Ed., Amer. Meteor. Soc., 139–213.
- Trenberth, K. E., 1991: Storm tracks in the Southern Hemisphere. *J. Atmos. Sci.*, **48**, 2159–2178.
- Van Bebber, W. J., 1882: Typische Witterungserscheinungen. Archiv der Dt. Seewarte Hamburg, 5. Jg., Nr. 3, 45 pp.
- , 1891: Die Zugstraßen der barometrischen Minima nach den Bahnenkarten der Deutschen Seewarte für den Zeitraum 1875–1890. *Meteor. Z.*, **8**, 361–366.
- Wallace, J. M., G.-H. Lim, and M. L. Blackmon, 1988: Relationship between cyclone tracks, anticyclone tracks, and baroclinic waveguides. *J. Atmos. Sci.*, **45**, 439–462.
- Washington, W. M., and G. A. Meehl, 1984: Seasonal cycle experiments on the climate sensitivity due to a doubling of CO<sub>2</sub> with an atmospheric general circulation model coupled to a simple mixed layer ocean model. *J. Geophys. Res.*, **89**(D6), 9475–9503.
- Whittaker, L. M., and L. H. Horn, 1982: *Atlas of Northern Hemisphere Extratropical Cyclone Activity, 1958–1977*. Dept. of Meteorology, University of Wisconsin, 65 pp.
- Williamson, D. L., 1981: Storm track representation and verification. *Tellus*, **33**, 513–530.
- Zapotocny, J. V., 1991: Trends in North America sector cyclogenesis (1958–1988) related to variations in mid-tropospheric standing wave amplitudes. Proc. of the 15th Annual Climate Diagnostic Workshop. National Climatic Data Center, NESDIS, NOAA, Asheville, NC., 108–113.
- Zishka, K. M., and P. J. Smith, 1980: The climatology of cyclones and anticyclones over North America and surrounding ocean environs for January and July, 1950–1977. *Mon. Wea. Rev.*, **108**, 387–401.